Fabrication and Analysis of High-Contrast InGaAsP–InP Mach–Zehnder Modulators for Use at 1.55-μm Wavelength

M. Fetterman, C.-P. Chao, and S. R. Forrest

***Abstract*— A high-contrast ratio, low voltage-length product, multiple quantum well InGaAsP–InP Mach–Zehnder interferometer is demonstrated and analyzed. An on/off ratio of over 40 dB and voltage-length product of 1.8 V-mm were measured, results which are superior to previous reports of similar MQW structures. Using the Lanczos–Helmholtz beam propagation method, we find that the linear and quadratic electrooptic coefficients for InGaAsP quantum wells are $r = (3.9 \pm 1.7)$ pm/V and $s = (5.0 \pm 1.5) \times 10^{-19}$ m²/V², respectively. We also demonstrate active optical alignment of the modulator guides using integrated waveguide light emitting diodes.**

I. Introduction

High-frequency modulation at a wavelength of $\lambda = 1.55$ μm is important for telecommunications and data communications [1]. External modulators such as the Mach–Zehnder (MZ) interferometer can operate at high frequencies, and can have relatively low chirp. Commercial MZ's are generally made from bulk $LiNbO_3$ crystals. On the other hand, semiconductor multiple quantum well (MQW) devices [2]–[5] that utilize the quantum confined Stark effect (QCSE) have a larger electrooptic coefficient than devices made from lithium niobate [6], leading to low switching voltages, reduced power consumption, and high bandwidths. Semiconductors also offer the potential for integration with other active optoelectronic components [7].

In this letter, a high-contrast ratio, low voltage-length product InP/InGaAsP MZ for use at a wavelength of $\lambda = 1.55$ μm is demonstrated. The 300-μm long device has a 6 V switching voltage, a switching voltage-length product of $V \cdot L = 1.8$ V-mm, and an on/off ratio $R > 40$ dB. These parameters, to our knowledge, exceed those reported to date [2]–[5]. The high R value of this MZ is due to low absorption loss and balanced splitting between the arms of the Y-branches (YB's), and the low $V \cdot L$ product is a consequence of the strong electrooptic effect in the InGaAsP guiding layers and quantum wells. To accurately analyze this device, we apply and extend the Lanczos–Helmholtz Beam Propagation Method [8] (LHBPM) to calculate the optical overlap factor, and to study the splitting [9] in the arms of the YB. In addition, we introduce alignment electrodes which consist of light-emitting diodes (LED's) on the input and output of the modulator waveguides. They simplify the task of aligning the MZ waveguides with input and output optical fibers, and are useful for packaging and fiber pigtailing.

Manuscript received June 21, 1995; revised September 6, 1995.

The authors are with the Department of Electrical Engineering, Advanced Technology Center for Photonics and Optoelectronic Materials, Princeton University, Princeton, NJ 08544 USA.

Publisher Item Identifier S 1041-1135(96)00545-9.

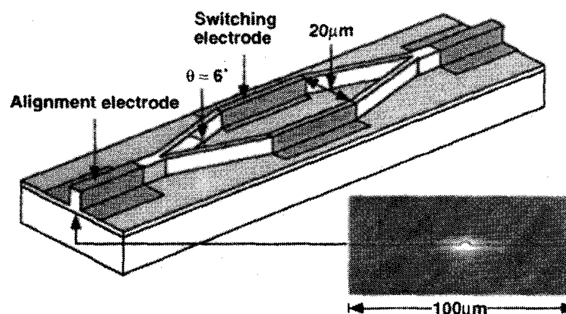

Fig. 1. Perspective schematic view of the Mach–Zehnder modulator. **Inset.** Image of the light spot emitted from an alignment electrode. Dimensions of the guided light from the electrode are on the order of (10 μm)^2.

The MZ modulator structure, shown schematically in Fig. 1, has two YB's with a 6° separation angle, a 3 μm wide waveguide ridge, and active lengths that vary from 300–700 μm. The center-to-center spacing of the electrode arms is 20 μm, and the total device length is 2.5 μm. The alignment electrodes allow for active fiber alignment to the waveguide by forward biasing light emitting diodes (LED's) at both ends of the MZ. By placing a detector at the opposite end of the fiber pigtail, the MZ waveguide can be rapidly and accurately aligned to the output fiber. The light intensity pattern emitted from one of these diodes is shown in the inset of Fig. 1, and the dimensions of the light spot are on the order of 10 μm, clearly indicating guiding of the emitted light in the ridge region.

The wafer was grown by metalorganic chemical vapor deposition on (100) n^+ InP S-doped at 10^{18} cm^{-3}. The first layer is a 1-μm thick, S:InP buffer layer also doped to 10^{18} cm^{-3}, followed by a 0.1-μm thick, undoped InGaAsP cladding layer with an energy gap of $E_g = 1.08$ eV. The undoped quantum well region consists of 5 unstrained InGaAsP ($E_g = 0.90$ eV), 70-Å thick quantum wells, and 100-Å thick barriers with $E_g = 1.08$ eV. A second undoped, 0.1-μm thick InGaAsP buffer layer ($E_g = 1.08$ eV), a Zn:InP (5×10^{17} cm^{-3}) 1-μm thick waveguiding layer, and a 0.2-μm thick, Zn:InGaAs layer (10^{19} cm^{-3}) for ohmic contact are grown on top.

1041-1135/96$05.00 © 1996 IEEE

To fabricate the waveguide device, a 1000-Å thick layer of SiN_x is deposited using plasma enhanced chemical vapor deposition at a substrate temperature of 250 °C. The SiN_x is then patterned as a 3-μm wide ridge etching mask. A 0.85 μm deep InGaAs–InP ridge was formed by reactive ion etching in a 550 V, CH_4–H_2 (1:6) plasma. Next, a 3000 Å thick SiN_x contact isolation layer is deposited, and then removed prior to e-beam deposition of Ti–Pt–Au (200 Å/500 Å/3000 Å) electrodes. After the wafer was lapped to a thickness of 150 μm, a Ge–Au–Ni–Au (270 Å/450 Å/215 Å/1200 Å) n-metal contact was deposited on the substrate surface and the contacts were annealed at 360 °C for 90 s. The wafer was then cleaved into rows of devices, and a 1800-Å thick SiO anti-reflective layer was e-beam evaporated onto the cleaved facet surfaces.

Fig. 2 shows the (TE mode) MZ output intensity as a function of voltage for a 300-μm long device, indicating $R > 40$ dB (limited by the output detector sensitivity), and a switching voltage of 6 V, giving $V \cdot L = 1.8$ V-mm. In contrast, the TM mode had $R = 5$–10 dB. Modulators with lengths ranging from 300–700 μm showed similar performance of $R = 30$–40 dB and $V \cdot L$ in the range of 1.8–4 V-mm for TE modes. For comparison [3], similar GaAs–AlGaAs MZ devices have $R =$ 23.8 dB and $V \cdot L = 5.5$ V-mm. InP–InGaAsP quantum well [2] MZ's have been demonstrated with $V \cdot L = 2.1$ V-mm and $R = 16$ dB. The fiber-to-fiber loss was measured to be 40 dB which is higher than the 31-dB insertion loss reported for a similar GaAs–AlGaAs MZ modulator using 1° Y-branches [3]. The higher loss is attributed, in part, to the larger branching angle of 6° used in this work. Also, some additional loss may be incurred due to the nonideal fiber-waveguide coupling of our experimental setup.

The capacitance and resistance of 300-μm long devices are 3.5 pF and 30 Ω, respectively. From these values, we estimate a 3-dB cut-off frequency of 1.5 GHz. However, the capacitance can be reduced by more than a factor of ten (and the frequency increased by a concomitant amount) by reducing the size of the electrode probing pads [3] and isolating the active and passive waveguide ridge regions.

The electroluminescence measured from the alignment electrode peaked at $\lambda = 1.32$ μm, implying that the absorption loss at the operating wavelength of $\lambda = 1.55$ μm is negligible. The data of Fig. 2 can, therefore, be fit using:

$$I(V) = I_0\{A^2 + B^2 + 2A^2B^2 \cos[\Delta n(V)kL + \phi]\}. \quad (1)$$

Here, $I(V)$ is the output intensity as a function of voltage, I_0 is the intensity at $V = 0$, $\Delta n(V)$ is the change of index of refraction as a function of voltage, $k = 2\pi/\lambda$, L is the device length, and ϕ is a phase shift. The two YB's are characterized by the coefficients A and B, where A and B are the intensities that couple into each arm following $A + B = 1$. The on/off ratio is then given by $R = 1/(A - B)^2$. For an on/off ratio of $R = 10^4$ as shown in Fig. 2, this implies that $A - B =$ 0.01, from which we infer a YB asymmetry of <1%. With (1), and using $A = B = 0.5$, $\Delta n(V)$ is extracted from the fit to the data of Fig. 2. The dependence of Δn on voltage and the corresponding theoretical fit are shown in the inset to Fig. 2.

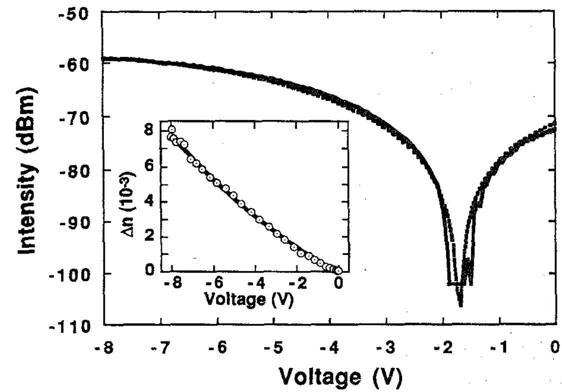

Fig. 2. The response of a 300 μm long Mach–Zehnder at $\lambda = 1.55$ μm. The on/off ratio is >40 dB and the switching voltage is 6 V. Dashed line is a theoretical fit to the data described in the text. Inset: Refractive index change, $\Delta n(V)$, obtained from the data of Fig. 2 (circles). Dashed line is a theoretical fit.

The index change is due to both the bulk (non-QW), Δn_{bulk}, and quantum well regions, Δn_{qw}, via $\Delta n = \Delta n_{qw} + \Delta n_{\text{bulk}}$. The value of Δn_{bulk} is [10]:

$$\Delta n_{\text{bulk}} = \tfrac{1}{2}\Gamma_{\text{bulk}}\, n_0^3\, [r_{\text{bulk}}\,(E - E_0) + s_{\text{bulk}}\,(E - E_0)^2 + (r_{\text{bulk}}E_0 - s_{\text{bulk}}E_0^2)], \quad (2)$$

where Γ_{bulk} is the optical confinement factor for the bulk region, n_0 is the refractive index with no applied field [11], r_{bulk} and s_{bulk} are the linear and quadratic electrooptic coefficients, respectively, E is the applied electric field, and E_0 is the built-in junction electric field. The same form of expression is also used for Δn_{bulk}.

To accurately determine Γ, and hence, the coefficients r and s, the LHBPM[8] was used to model the waveguide modes and YB splitting of the MZ. An exact solution of the Helmholtz equation used in modeling wave propagation generally considers the set of all possible waves propagating at each point of a grid in the x–y plane perpendicular to the propagation direction, z, using a coupling matrix. However, this is often not possible to implement since grids consisting of the large number of points necessary to model structures with a complicated index profile, $n(x, y)$, such as the MQW MZ, require an extremely large coupling matrix. The LHBPM reduces the original extremely large coupling matrix to a subspace that only has a few elements, making the wave propagation problem soluble. In our calculations we used the wafer structure previously described with the following refractive indices [11]: $n_{\text{sub}} = 3.17$ (InP substrate), $n_{\text{barrier}} = 3.30$ (the InGaAsP cladding region and quantum well barriers are made of the same material), and $n_{qw} = 3.46$ (InGaAsP quantum wells) along with a five-dimensional Lanczos subspace. Grid spacings of $\Delta x = 0.15$ μm, $\Delta y = 25$ Å, and a propagation step increment of $\Delta z = 1$ μm were used. Often when modeling such structures, the index of refraction is taken to be the average of the quantum well and barrier materials. Here, the resolution of the grid was sufficient so that this approximation was not necessary.

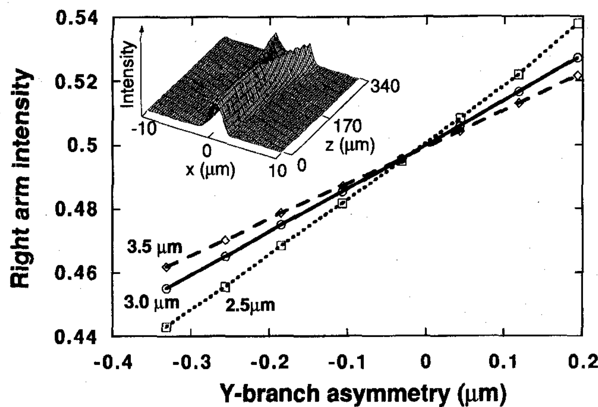

Fig. 3. The calculated fraction of power coupled into the right arm as a function of the difference in widths of an asymmetric Y-branch. The left arm is held fixed at the width indicated, and the right arm width is varied. Inset: Light intensity showing propagation in an asymmetric Y-branch.

Optical confinement factors of $\Gamma_{\text{bulk}} = 0.54$ and $\Gamma_{qw} = 0.12$ were calculated by the LHBPM. Previous work [2] has shown that $s_{\text{bulk}} = 0$ and that $r_{qw} = r_{\text{bulk}}$. With these assumptions and the data from the inset of Fig. 2, it is found that $r_{qw} = r_{\text{bulk}} = (3.9 \pm 1.7)$ pm/V and $s_{qw} = (5.0 \pm 1.5) \times 10^{-19}$ m^2/V^2. The dotted line in Fig. 2 fits the experimental data assuming these values for r and s and (1) and (2). This fit also gives $V_\pi = 6$ V. By comparison, the linear electrooptic coefficient of bulk GaAs[10] at $\lambda = 1.15$ μm is $r_{\text{bulk}} = 1.6$ pm/V and the quadratic electrooptic coefficient of a similar GaAs QW device [3] at $\lambda = 0.8$ μm is $s_{qw} = 1.3 \times 10^{-18}$ m^2/V^2.

The LHBPM was also used to study the coefficients A and B of the YB's [9], defined in (1). Fig. 3 shows the ratio of power coupled into the right YB arm as a function of the arm width difference, or YB waveguide asymmetry. The inset to Fig. 3 shows a plot of wave intensity as a function of position in a YB. In Fig. 3, the three curves correspond to waveguide widths of $W = 2.5$ μm, 3.0 μm, and 3.5 μm. The difference between the slope of the curves shows that, as expected, YB's constructed using wide waveguides are less sensitive to asymmetries than are narrow guides. When the width of the 3 μm guide used in our devices varies by 0.04 μm, then $A - B = 0.01$, implying that >40 dB on/off ratio is possible under these circumstances. Besides using balanced Y-branches, to achieve a high on/off ratio we also need to minimize voltage induced absorption changes which can lead to asymmetries in the intensity of the two waves at the output Y-branch. To accomplish this, we have a QW with an effective energy gap of 0.9 eV, which is further from the 1.55 μm operational wavelength than is typical for MQW MZ modulators [4]. In addition, operation far from the band edge accounts for the apparently low-quadratic electrooptic coefficient in our device. Nevertheless, at an operational voltage of 3 V, about one third of the total index change comes from the quadratic electrooptic effect.

In conclusion, we fabricated and analyzed a high-contrast ratio, low switching-voltage InGaAsP MQW MZ modulator for use at $\lambda = 1.55$ μm. A 300 μm long device has a 6 V switching voltage, $V \cdot L = 1.8$ V-mm, and $R > 40$ dB. These parameters, to our knowledge, exceed those reported to date [2]–[4]. The electrooptic coefficients of the InGaAsP QW material were measured and analyzed using the highly accurate Lanczos–Helmholtz beam propagation method, and are found to be $r = (3.9 \pm 1.7)$ pm/V and $s = (5.0 \pm 1.5) \times 10^{-19}$ m^2/V^2 for the linear and quadratic electrooptic coefficients at 1.55 μm, respectively. Effects of waveguide asymmetry are also studied using this model. The high R-value of this MZ is due to low-absorption loss and extremely even splitting between the arms of the YB's. We demonstrate novel active waveguide input/output electrodes, which make fiber alignment to waveguide devices faster and more accurate than current passive alignment methods.

ACKNOWLEDGMENT

The authors thank US Army CECOM and ARO for their support of this work.

REFERENCES

[1] A. B. Buckman, *Guided-Wave Photonics.* Orlando, FL: Saunders College Publishing, 1992.

[2] J. E. Zucker, K. L. Jones, B. I. Miller, and U. Koren, "Miniature Mach–Zehnder InGaAsP quantum well waveguide interferometers for 1.3 μm," *IEEE Photon. Technol. Lett.*, vol. 2, pp. 1041–1043, 1990.

[3] S. Cites and P. R. Ashley, "High-performance Mach–Zehnder modulators in multiple quantum well GaAs/AlGaAs," *J. Lightwave Technol.*, vol. 12, pp. 1167–1173, 1994.

[4] N. Agrawal, D. Franke, C. M. Weinert, H.-J. Ehrke, G. G. Mekonnen, D. Franke, C. Bornholdt, and R. Langenhorst, "Fast 2 × 2 Mach–Zehnder optical space switches using InGaAsP-InP multiquantum-well structures," *IEEE Photon. Technol. Lett.*, vol. 7, pp. 644–645, 1995.

[5] K. Wakita, I. Kotaka, and H. Asai, "High-speed InGaAlAs/InAlAs multiple quantum well electrooptic phase moduators with bandwidth in excess of 20 GHz," *IEEE Photon. Technol. Lett.*, vol. 4, pp. 16–18, 1992.

[6] T. Fujiwara, A. Watanabe, and H. Mori, "Measurement of uniformity of driving voltage in Ti:LiNbO$_3$ waveguides using Mach–Zehnder interferometers," *IEEE Photon. Technol. Lett.*, vol. 2, pp. 260–262, 1990.

[7] T. L. Koch, "Semiconductor photonic integrated circuits," *J. Quantum Electron.*, vol. 27, pp. 641–643, 1991.

[8] R. P. Ratowsky and J. A. Fleck, Jr., "Accurate numerical solution of the Helmholtz equation by iterative Lanczos reduction," *Opt. Lett.*, vol. 16, pp. 787–789, 1991.

[9] H. P. Chan, P. S. Chung, and E. Y. B. Pan, "Mode conversion in Y-branch waveguides," in *SPIE, Integrated Optical Circuits*, vol. 1583, pp. 129–132, 1991.

[10] A. Yariv and P. Yeh, *Optical Waves in Crystals.* New York: Wiley, 1983.

[11] B. Broberg and S. Lindgren, "Refractive indices of InGaAsP," *J. Appl. Phys.*, vol. 55, pp. 3376–3381, 1984.